# Topographic and orbital forcing of Titan's hydroclimate

Juan M. Lora[a,*], J. Michael Battalio[a], Mary Yap[a] and Colin Baciocco[a]

[a]*Department of Earth and Planetary Sciences, Yale University, New Haven, CT, USA*

ARTICLE INFO

*Keywords*:
Titan
Titan, atmosphere
Titan, hydrology
Titan, surface
Meteorology

ABSTRACT

The cause of the hemispheric asymmetry of Titan's methane lakes and seas is the subject of ongoing debate. A leading hypothesis posits that seasonal insolation asymmetries caused by Saturn's eccentric orbit lead to differences in net precipitation over the two poles, perhaps mediated by asymmetric atmospheric transport of moisture. But topographic variations have also been proposed to contribute, albeit without considering the importance of surface hydrology. Here we present general circulation model simulations including a synchronously coupled surface and ground hydrology scheme, testing the separate and combined influences of topography and orbital forcing on Titan's hydroclimate. We find that, while topography leads to warmer polar regions relative to a flat surface which in turn enhances methane loss to the atmosphere, the overall effect on the global distribution of surface methane liquid is minor. In particular, topography does not force any notable asymmetry in the meridional circulation, nor does it affect the seasonality of the methane cycle, though it does increase the regional heterogeneity of average precipitation at mid-latitudes. We also find that Titan's atmospheric methane transport robustly responds to orbital forcing, in agreement with previous results, but this is insufficient to overcome the distribution of surface liquids dictated by surface hydrology. We conclude that Croll-Milankovitch cycles are plausible on Titan, but likely not the dominant driver of the current distribution of liquids; relatedly, our results suggest that the volume of the large seas and lakes has not varied substantially on millennial timescales.

## 1. Introduction

Titan supports an active hydrologic cycle, comprising observed features like clouds, rivers, lakes, and seas (Roe, 2012; Turtle et al., 2011a, 2018b; Hayes, 2016; Lopes et al., 2019), in which methane cycles through the atmosphere and crust on various timescales (Lunine and Lorenz, 2009; Roe, 2012; Mitchell and Lora, 2016; Hörst, 2017; Hayes et al., 2018). Titan's sporadic cloud activity evolves seasonally, and summer clouds have now been observed at the high latitudes of both hemispheres (Turtle et al., 2018b). These polar regions host surface lakes and seas of liquid methane (Hayes, 2016), some of whose shorelines have potentially retreated on sub-annual timescales (Turtle et al., 2011b; Hayes et al., 2011; MacKenzie et al., 2019a).

Separately, general circulation models (GCMs) of Titan have demonstrated that the climate system transports methane to the polar regions on multi-annual timescales, where liquid is cold-trapped in the surface reservoirs (Mitchell, 2008; Schneider et al., 2012; Lora et al., 2015; Newman et al., 2016). And, conversely, simulations with ample surface methane at the polar regions—beyond that available in the seas and lakes—best reproduce various aspects of the observed hydroclimate (Lora and Mitchell, 2015; Mitchell and Lora, 2016; Lora and Ádámkovics, 2017; Faulk et al., 2017). (Geologic and remote sensing evidence similarly points to wet polar surfaces (e.g., Neish and

*Corresponding author
juan.lora@yale.edu (J.M. Lora)
ORCID(s): 0000-0001-9925-1050 (J.M. Lora)

Lorenz, 2014; Jennings et al., 2016).) Methane moisture, sourced at the poles, humidifies the lower latitudes via the atmospheric circulation (Griffith et al., 2014; Mitchell and Lora, 2016; Lora and Ádámkovics, 2017; Battalio and Lora, 2021).

On longer timescales, orbital precession causes the seasonal insolation asymmetry due to Saturn's orbital eccentricity to evolve on roughly $10^4$ year timescales, and this has been proposed to contribute to or control the asymmetric distribution of the surface liquids: Titan's large seas and the vast majority of small lakes occur in the north (Aharonson et al., 2009; Hayes, 2016). Indeed, Lora et al. (2014) showed that a surface methane difference between hemispheres in four paleoclimate GCM simulations corresponded to the hemispheric contrast in peak insolation caused by changes in orbital parameters. Other studies have similarly found that the modern orbital configuration, with perihelion occurring close to northern summer solstice, leads to a net accumulation of methane in the north (Schneider et al., 2012; Lora et al., 2015; Lora and Mitchell, 2015; Newman et al., 2016). Lora and Mitchell (2015) further showed that equatorward transport by atmospheric eddies is asymmetric, providing a mechanism to translate the asymmetric seasonal forcing into a net transport by the atmosphere.

Surface observations of Titan, however, do not lead to an unequivocal interpretation in agreement with these findings. Geomorphologic mapping of Titan's polar regions suggests that roughly equal areas in the two hemispheres are made up of low-lying basins, which are filled in the north but empty in the south, suggestive of paleo-seas (Birch et al., 2017, 2018). But putative evaporitic deposits, present extensively in the northern basins and shores of filled lakes (as well as at lower latitudes), are conspicuously absent from the southern polar regions (MacKenzie et al., 2014). Therefore, if methane cycles between poles on the timescale of precessional cycles, then evaporites left behind in the south would need to have been buried or removed, implying that a complete emptying of southern lakes and seas is not occurring at present and thus should have occurred relatively quickly in the recent past. A clear alternative is that such liquids never existed in the past $\sim 10^4$ years, obviating the need for a net pole-to-pole transport mechanism, and that basin formation was much more ancient.

Moreover, all of the above GCM studies used simplified approximations for surface hydrology and ignored the influence of topography, disregarding, for example, the importance of runoff. Such simplifications could be important, particularly given the substantial surface–atmosphere interactions and associated feedbacks. More recently, Tokano (2019) used a GCM incorporating heterogeneous surface properties (topography, albedo, emissivity, and thermal inertia) to suggest that an asymmetric meridional circulation, forced in particular by surface topography, hinders precipitation in the southern hemisphere and is therefore the principal driver of any asymmetry. This would suggest that Titan's lake distribution resists any influence of orbital forcing, and thus may not have changed significantly on $<10^5$ year timescales.

Yet the study of Tokano (2019) also used a simplified hydrology scheme, neglecting lateral transport of surface liquids; surface methane was exclusively affected by precipitation and evaporation. On the other hand, Faulk et al. (2020) recently coupled a hydrology model and GCM, enabling for the first time a fully self-consistent simulation of the methane cycle that demonstrated the importance of subsurface methane in enabling high-latitude surface moisture. However, that model did not explicitly account for the direct influence of topography on the atmosphere, so evaluation of such influence on the resulting meridional circulation was not possible.

The present study addresses that gap. Here, we present new simulations with the coupled GCM and hydrology model (Faulk et al., 2020), wherein topography now interacts fully with the atmosphere. We evaluate the influence of this interaction in the context of the hydroclimate including surface and subsurface hydrology. And, using our updated model, we test the relative importance of orbitally-forced seasonal insolation asymmetries in the global transport of methane, and the consequent distribution of lakes and seas.

## 2. Methods

The model we use in this study is a configuration of the Titan Atmospheric Model (TAM; Lora et al., 2015). TAM is a three-dimensional GCM based on the GFDL Flexible Modeling System, which, in addition to its spectral dynamical core, uses component modules to parameterize unresolved physical processes including moist convection, large-scale condensation, surface heat conduction, surface–atmosphere fluxes, turbulent diffusion, and full radiative transfer (Lora et al., 2015; Lora and Ádámkovics, 2017; Lora et al., 2019). We run the model at T21 resolution (64 longitude by 32 latitude grid points), with 24 unevenly spaced vertical levels, and a time-step of 600 s. In all cases, we use a constant surface thermal inertia of 750 J $m^{-2}$ $s^{0.5}$ $K^{-1}$ (MacKenzie et al., 2019b). In addition, we employ several recent updates including a tuned convection parameterization and other incremental improvements (Battalio et al., 2021) and, crucially, a model of surface and subsurface methane hydrology that enables the self-consistent simulation of the methane cycle (Faulk et al., 2020).

The hydrology model, which calculates infiltration, runoff, and a subsurface methane table with lateral flow, uses topography as an input (Faulk et al., 2020). Here, we additionally incorporate the direct effects of topography on Titan's atmosphere by including it as a lower boundary condition in selected simulations. To accomplish this, we use the geoid-corrected map of Titan's topography estimated from Cassini RADAR data (Corlies et al., 2017), slightly modified to enforce a flat equipotential surface over Titan's maria. In addition, we do not regularize the topography. For consistency, we use the same topography as a boundary condition for both the atmosphere and for the hydrology model, and as a result the latter is somewhat different than that in Faulk et al. (2020); the large-scale features are nevertheless equivalent.

For this work, we run a number of simulations to investigate the individual and cumulative effects of the topography and of orbital forcing variations on Titan's hydroclimate. First, we run four simulations that use 1) either a flat surface (as in previous studies) or the new topography, and 2) either Saturn's modern orbital parameters or a case with the longitude of perihelion shifted by 180° with respect to modern. (This latter forcing causes the shorter, more intense summer to occur in the northern hemisphere, while other orbital parameters are held constant; this is slightly different than the approach used by Lora et al. (2014), but roughly corresponds to their 28-kyr-before-present case.) The simulations are otherwise identical. We note, in particular, that in all cases the hydrology model uses the input topography as a prerequisite for calculating runoff and seepage; in other words, only the lower atmospheric boundary condition is flat in the "flat surface" simulations, as in Faulk et al. (2020).

In all four of these cases, we use a value for the hydraulic conductivity of the surface $k = 5 \times 10^{-5}$ m s$^{-1}$ within the hydrology model based on previous results with a flat surface (Faulk et al., 2020). We find, however, that while our flat simulations behave as expected, the simulations using topography begin to lose their surface liquid methane after about four decades, and thus do not trend toward a statistical equilibrium that corresponds to Titan's observed surface. As a result, we run two additional simulations (one each for the two longitude of perihelion configurations) with topography and with a higher hydraulic conductivity $k = 10^{-4}$ m s$^{-1}$. These are restarted from the end of the 40th Titan year of the corresponding lower-$k$ simulations with topography.

In all cases, simulations are run out to the 100th year (henceforth, references to "years" and "decades" correspond to Titan years), and all comparisons between simulations that follow are done using corresponding years (unless otherwise noted, figures show results from the final decade of simulations). Simulations are initialized at year zero using no surface liquid and a prescribed amount of subsurface methane, as in Faulk et al. (2020), as well as with a previously spun-up atmospheric state to minimize computational expense. All simulations reach statistical steady state for relevant atmospheric variables, like temperature, winds, and humidity, within 20 years. While there is still some interannual variability in, for example, the total surface liquid by the 100th year, we find that our results are robust when using multiple years (and this allows an estimate of uncertainty due to variability). The exception, of course, is the pair of simulations (with topography and $k = 5 \times 10^{-5}$ m s$^{-1}$) mentioned above, which consistently lose surface methane in the final several decades.

# 3. Results

## 3.1. Impact of topography

We begin by investigating the impact of topography as a boundary condition for the atmosphere in the simulations using Titan's modern effective orbital configuration (in other words, Saturn's orbit around the Sun). The principal questions motivating this are whether the topography introduces any substantial structure into hydroclimate patterns,

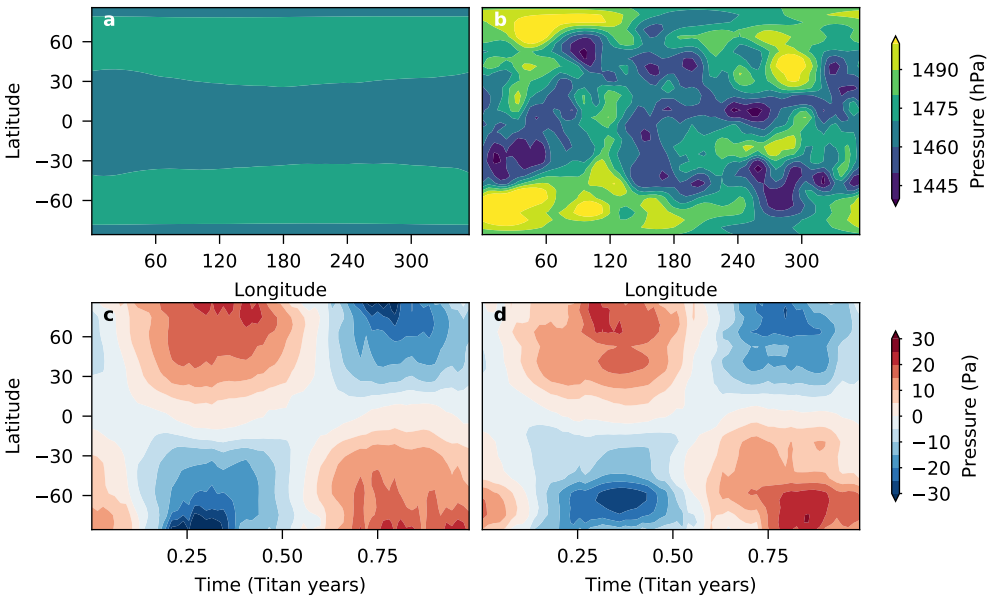


**Figure 1:** Surface pressures. Top: time-averaged surface pressures for simulations (a) without and (b) with topography. Bottom: climatological seasonal evolution of zonally averaged anomalous surface pressure for simulations (c) without and (d) with topography. The beginning of the year corresponds to northern autumnal equinox.

and whether or not it instigates a significantly asymmetric Hadley circulation as it does on Mars (e.g., Richardson and Wilson, 2002; Zalucha et al., 2010).

The annually-averaged surface pressure, as well as its climatological (i.e., the decadal average) seasonal anomalies, from simulations with and without topography, are shown in Fig. 1. Immediately apparent is the fact that topography leads to large variations of the average surface pressure—on the order of tens of hPa—on regional scales, corresponding to the distribution of valleys and ridges of the surface. Indeed, because the low-lying basins cluster at higher latitudes, the surface pressure tends to be higher near the poles and lower over the low-latitude highlands, with the exception of the region of Xanadu (roughly 20°S, 240–300°E), which is thought to be relatively low-lying, albeit mountainous (Lorenz et al., 2013; Corlies et al., 2017). All of this is in stark contrast to the case without topography, wherein the average surface pressure variations are very weak.

On the other hand, seasonal surface pressure anomalies are small for both simulations (on the order of tens of Pa between summer and winter at the poles), consistent with Titan's weak Coriolis force and temperature gradients (Mitchell and Lora, 2016). Importantly, these anomalies are also effectively indistinguishable between simulations, indicating that topography has little meaningful impact on the movement of mass in Titan's atmosphere.

Consistent with this, the climatological seasonal anomalies of surface temperature (Fig. 2a, d) and column-integrated methane (Fig. 2b, e) are also largely interchangeable between simulations, showing no appreciable difference

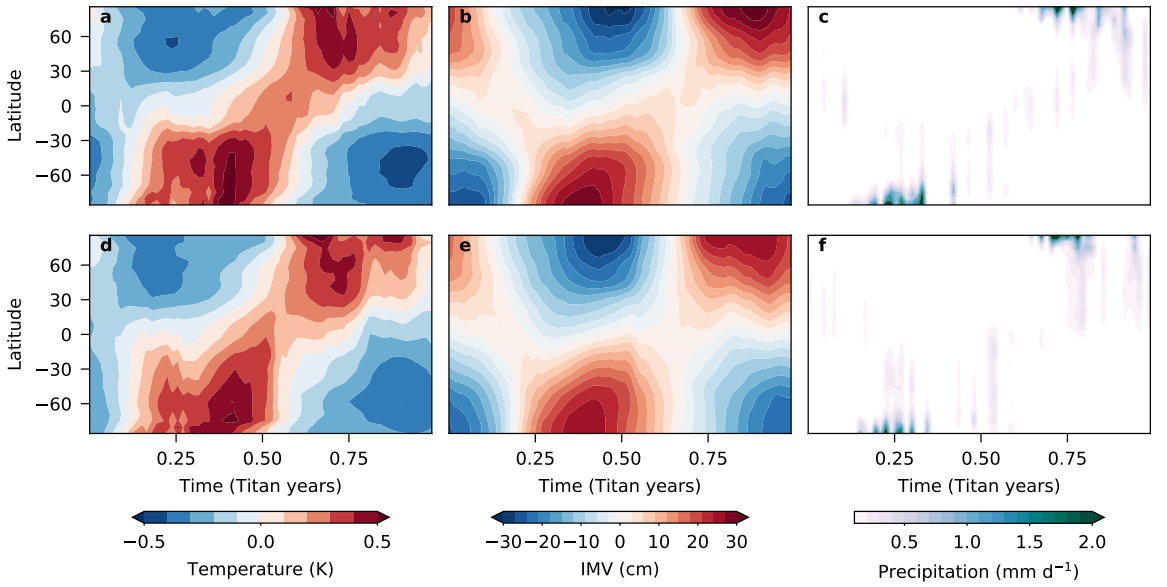


**Figure 2:** Seasonal variations. Climatological seasonal evolution of zonally averaged (a, d) anomalous surface temperatures, (b, e) anomalous column-integrated atmospheric methane vapor (IMV), and (c, f) precipitation, for simulations (a–c) without and (d–f) with topography (in f, the case with $k = 10^{-4}$ m s$^{-1}$ is shown). The beginning of the year corresponds to northern autumnal equinox.

either in magnitude or timing. These diagnostics indicate that, while topography affects the time-averaged distribution of atmospheric mass (as expected, since there is less atmosphere over a tall mountain, for instance) and correspondingly the column methane vapor at any one location, it does little to modify Titan's seasonal circulation patterns and humidity variations relative to the well-studied case without topography.

Comparison of the seasonality of zonally-averaged precipitation between analogous simulations with topography (that is, simulations in which the methane cycle is equally active; see Section 2) similarly shows almost no differences (Fig. 2c, f): precipitation peaks over the summer poles and occurs sporadically at other latitudes, with a slight but consistent enhancement at northern relative to southern latitudes during their respective summers. The single notable difference in precipitation distributions is the modest increase in southern midlatitude activity in early summer in the simulation with topography, which could be a better match to early observations of Titan's clouds (e.g., Roe et al., 2005) and will be further discussed below.

Figure 3 shows the climatological seasonal meridional mass stream function in Titan's lower atmosphere for the two simulations. As in previous studies, the model simulates a seasonal Hadley circulation with relatively strong, cross-equatorial winter cells and weak, shallow summer cells, accompanied by relatively steady and shallow thermally indirect cells at higher latitudes, which are associated with eddy activity (Lora and Mitchell, 2015). While quantitative

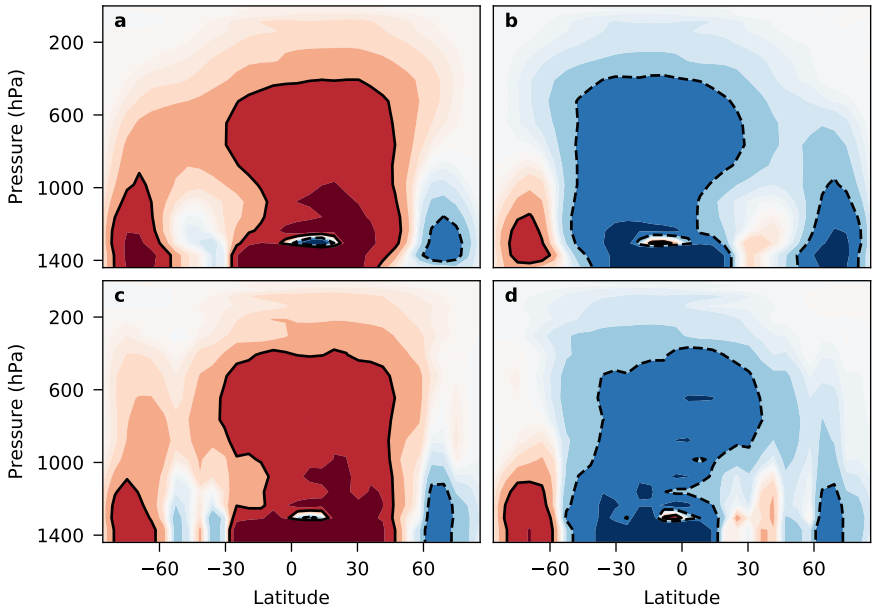


**Figure 3:** Meridional mass stream function. Time-averaged meridional mass stream functions over northern fall and winter (a, c) and northern spring and summer (b, d) for simulations (a, b) without and (c, d) with topography. Positive values indicate clockwise motion. Contours increase by factors of 2; the $\pm 0.5 \times 10^9$ kg s$^{-1}$ contours are shown in solid (positive) and dashed (negative) black contours.

differences exist, there is little indication of significant qualitative differences in the meridional circulation from the simulation with topography relative to the one without. In particular, we find no evidence of a hemispheric asymmetry induced by the topography. We therefore discard this as a plausible mechanism to drive the asymmetry of surface liquids on Titan.

Importantly, all of the above results do not mean that topography has *no* effect on Titan's hydroclimate. Consistent with the distribution of time-averaged surface pressures, the distribution of time-averaged surface temperatures is affected by the topography (Fig. 4): lower elevation surfaces are warmer than other regions as a simple consequence of the lapse rate. But because this principally affects higher latitudes, the ultimate result is that the equator-to-pole surface temperature difference is approximately 0.6 K smaller on average in the case with topography. This, in turn, means that the poles are weaker cold traps for surface liquid, which initially promotes a more vigorous methane cycle but, as described in the previous section, eventually leads to a loss of surface methane in the case with $k = 5 \times 10^{-5}$ m s$^{-1}$. Less surface and near-surface liquid leads to lower evaporation rates, which in turn causes higher surface temperatures (Mitchell, 2008; Lora et al., 2015; Lora and Ádámkovics, 2017; MacKenzie et al., 2019b); the result, after 100 years, is shown in Fig. 4b.

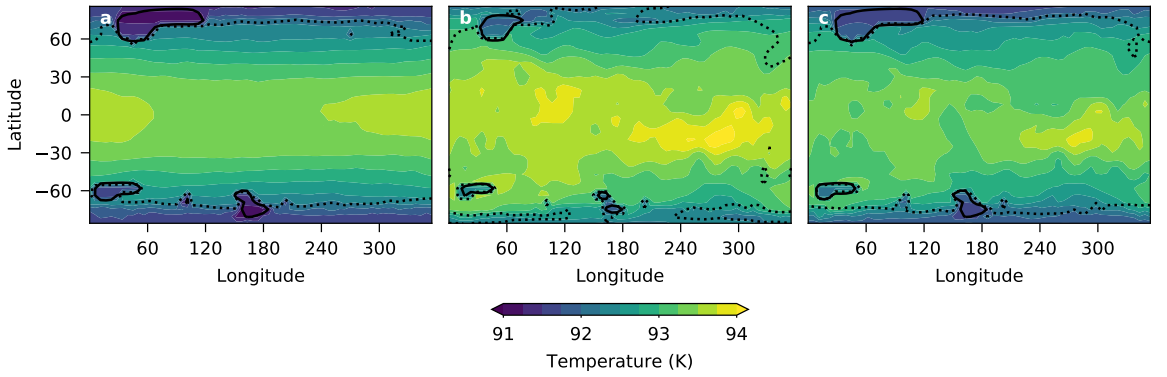


**Figure 4:** Surface temperatures. Time-averaged surface temperatures for simulations (a) without topography, (b) with topography, and (c) with topography and increased hydraulic conductivity. Locations with surface liquid methane exceeding 25 m are outlined in black solid contours; locations where average evaporation exceeds 0.1 mm $d^{-1}$ ("day" refers to Earth days) are outlined in black dotted contours.

Figure 4c shows the equivalent time-averaged surface temperatures for the simulation with topography and $k = 10^{-4}$ m $s^{-1}$. In this case, the higher hydraulic conductivity allows seepage of subsurface methane to offset atmospheric divergence of methane moisture from the high latitude surface sources, balancing the evaporation rates and allowing for a stable hydroclimate in the last several decades of simulation (see Fig. 2f). Under this configuration, the global average surface temperature is similar to the case without topography (Fig. 4), though still equator-to-pole contrasts are weaker, and the polar cold traps are therefore also weaker (Fig. 4a, c).

The corresponding distributions of surface and near-surface liquids for the final decade of the simulations are also illustrated in Fig. 4 (near-surface liquid is indicated by regions with substantial average evaporation rates). Interestingly, the total volume of surface liquids at the end of our simulations is on the order of $10^5$ $km^3$, in excellent agreement with the total volume of Titan's liquids estimated from observations (Lorenz et al., 2008; Mastrogiuseppe et al., 2014).

In all cases, surface liquids pool in areas of topographic lows corresponding to Titan's Kraken and Ligeia maria and the catchment basin of Ontario Lacus, as well as in the lowest-elevation basin in the southern hemisphere (around 60°S, 30°E), a location where liquids have not actually been observed. All of this is primarily due to the routing of runoff, in combination with the latitudinal balance of precipitation and evaporation (Faulk et al., 2020). Outside of these surface liquids, ample evaporation (from near-surface ground methane) occurs at high latitudes, corresponding to the subsurface methane reservoirs and moist regolith inferred in previous works (Neish and Lorenz, 2014; Lora and Mitchell, 2015; Mitchell and Lora, 2016; Jennings et al., 2016; Lora and Ádámkovics, 2017; Turtle et al., 2018b; Faulk et al., 2020).

In the simulation with topography and $k = 5 \times 10^{-5}$ m $s^{-1}$, surface liquids and high evaporation rates cover substantially smaller areas than in the flat case by the end of the simulations (Fig. 4b), consistent with a foundering

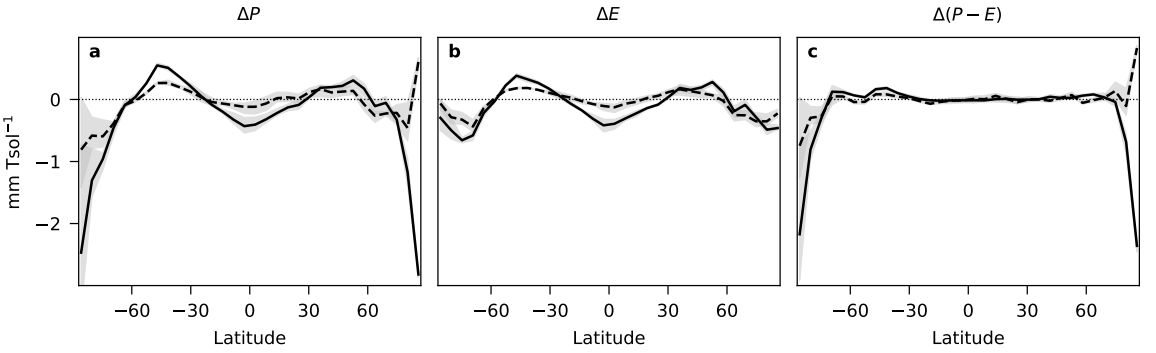


**Figure 5:** Responses of surface moisture fluxes to topography. Time- and zonal-mean differences in (a) precipitation, (b) evaporation, and (c) precipitation minus evaporation between simulations with and without topography (solid curves), as well as between simulations with topography plus increased hydraulic conductivity and without topography (dashed curves). In all cases, the gray shading shows the range of decadal averages over the final three decades of the simulations.

methane cycle. On the other hand, in the simulation with topography and $k = 10^{-4}$ m s$^{-1}$, Kraken/Ligeia Mare and Ontario Lacus, as well as regions with near-surface ground methane, are similar in area as in the flat case, while the other (unobserved) southern reservoir is smaller, therefore better approximating observations (Fig. 4c).

These points are further demonstrated by a quantification of precipitation and evaporation differences between the simulations. Fig. 5 shows the impacts of topography, as well as an estimate of uncertainty due to variability, from the final three decades of the simulations. Under the same hydraulic conductivity, topography leads to modest increases in average precipitation in the mid-latitudes, as well as a modest decline near the equator; the largest impact, however, is in substantial declines at higher latitudes, which approach 2 mm Tsol$^{-1}$ ("Tsol" refers to a Titan day) on average near the poles (Fig. 5a). With higher hydraulic conductivity, these differences are muted and, in particular, polar precipitation differences are smaller and of opposite signs in the north and south.

The evaporation response closely follows that of precipitation (Fig. 5b), since precipitation enables subsequent evaporation from lower latitudes, which are otherwise relatively dry. The exception is, expectedly, at higher latitudes, where ground methane is sufficiently close to the surface to provide a source of liquid (as illustrated in Fig. 4). Evaporation differences between the cases with and without topography suggest less polar evaporation in the former, as a result of the evaporation line being farther poleward; this is especially true for the case with lower hydraulic conductivity, as discussed above.

In the net, differences in surface–atmosphere fluxes of moisture largely cancel out at most latitudes, with the exception of the polar regions (Fig. 5c). There, the simulation with topography and lower hydraulic conductivity clearly has less net precipitation ($P - E$) than the flat case, which leads to the loss of surface methane described above. On the other hand, the simulation with topography and higher hydraulic conductivity has lower net precipitation in the south, but higher net precipitation in the north, than the flat case. In other words, this simulation has a slightly enhanced

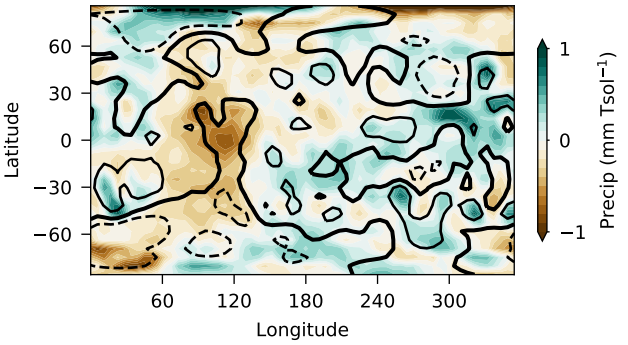


**Figure 6:** Zonally anomalous precipitation differences. Time-mean differences in the zonally anomalous (with the zonal average removed) precipitation between simulations with topography plus increased hydraulic conductivity and without topography, over the final three decades of the simulations. Topography is indicated by black contours, with solid and dashed contours indicating values 300 m above and below the average, which is shown in bold.

hemispheric asymmetry in net precipitation due to topography, although, as seen in Fig. 4, this is only barely reflected in the surface liquids. We note that, on average, the southern polar surface has slightly lower elevations than does the northern, and at the same time the deepest basin occurs more equatorward than do the deep basins of the north. In combination, these properties result in a modestly weaker cold trap and therefore a strengthened north–south net precipitation asymmetry, but only in the case where hydraulic conductivity is high enough that polar surface liquids are stable over long periods. These impacts do not depend on asymmetries of the meridional circulation.

A distinct impact of the topography is that it introduces inhomogeneities on regional scales. Southern mid-latitude precipitation is enhanced relative to the flat case, as can be seen in Fig. 5a, and this is accompanied by a slight depression of precipitation at the equator. While the absolute magnitudes are modest, these changes correspond to a threefold enhancement at southern mid-latitudes and a nearly 100% depression at the lowest elevations near the equator. This reflects both the low totals in these regions, but also the important influence of topography on the occasional rainstorms that affect them. Indeed, at mid- and lower latitudes, regions of relatively low (high) precipitation occur in regions of relatively low (high) elevation (Fig. 6); this is particularly obvious at the equator and 120°E, as well as in the highlands surrounding Xanadu. Especially over the topographic rises around 40°S and between 180 and 330°E, precipitation is enhanced; these results constitute indications of orographic precipitation on Titan (see Barth, 2010), which merit further study. A possible geographic control of southern midlatitude clouds was suggested based on cloud observations early in Titan's southern summer (Roe et al., 2005), although this was later discounted. Our results here suggest that topography does in fact locally enhance precipitation (and, by extension, precipitating clouds, though we do not explicitly model cloudiness), although precipitation at the same latitudes also occurs at other longitudes. In short, precipitation is enhanced (depressed) over high (low) elevation and increases at mid-latitudes (in both hemispheres) as a result of topography, but none of this has obvious consequence on the distribution of surface liquids.

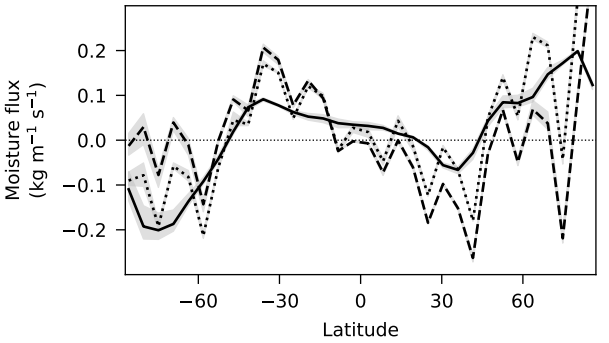


**Figure 7:** Meridional moisture fluxes. Time- and zonal-mean atmospheric fluxes of moisture from simulations without topography (solid curve), with topography (dashed curve), and with topography and increased hydraulic conductivity (dotted curve). In all cases, the gray shading shows the range of decadal averages over the final three decades of the simulations. Positive values indicate northward transport.

## 3.2. Impact of orbital forcing

Having established that the latitudinal distribution of surface liquids in our simulations with Titan's modern orbital configuration is largely determined by surface hydrology and only indirectly affected by the influence of topography on the atmosphere, we next turn to assessing the importance of orbital forcing on Titan's hydroclimate in the current version of TAM. The primary aim is to understand whether seasonal asymmetries due to the eccentricity of Saturn's orbit produce a first- or second- order effect in our atmosphere–surface coupled model.

As a starting point, the net atmospheric moisture fluxes from the three simulations with modern orbital configuration are shown in Fig. 7. In the case without topography, this consists of poleward moisture transport at high latitudes and equatorward transport at mid-latitudes, with a hemispheric asymmetry that results in cross-equatorial transport and convergence in the northern hemisphere; these results are quite similar to the idealized case described in Lora and Mitchell (2015), including in their magnitude. It is worth emphasizing that these represent the net transport that comprises the residual of much larger, mostly opposing cross-equatorial seasonal fluxes (Lora and Mitchell, 2015).

Topography introduces considerable noise into the net moisture flux curves (Fig. 7), which is due to the zonal averaging that also results in residuals from opposing fluxes. Nevertheless, the overall global signal is still apparent; the case with $k = 10^{-4}$ m s$^{-1}$ (dotted line) largely resembles the flat simulation, whereas the case with $k = 5 \times 10^{-5}$ m s$^{-1}$ (dashed line) produces generally more equatorward transport everywhere. In both cases, hemispheric asymmetries are difficult to see, though poleward transport is somewhat stronger at northern than southern high latitudes.

The total integrated northward transport of moisture in each simulation is shown in Fig. 8. With this metric, the impact of orbital forcing is more apparent, and the net atmospheric transport in the simulations coincides with expectations: northward in the modern, southward with a reversed perihelion, with approximately the same magnitude. However, this is only true when surface liquids are sufficiently stable (and available to evaporate): in the cases with

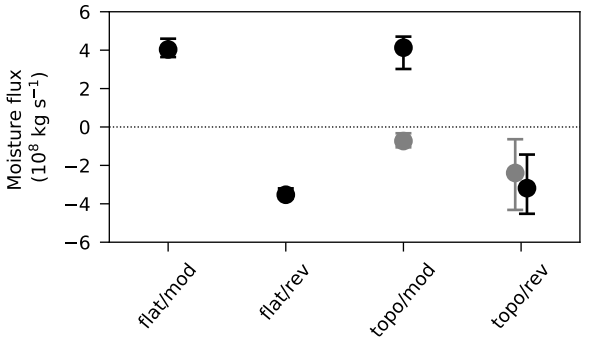


**Figure 8:** Net moisture transport. Net atmospheric moisture transport in each simulation: "Flat/topo" refers to simulations without or with topography, and "mod/rev" refers to the perihelion case, either modern or reversed. Gray symbols denote the results for the simulations with topography and lower hydraulic conductivity in which the surface liquids steadily decrease. Both the average and range of decadal averages over the final three decades of the simulations are shown. Positive values indicate northward transport.

topography and lower hydraulic conductivity (and disappearing surface liquids), the modern net transport is about zero. This latter point is an indication of the dependence of the orbital forcing mechanism (e.g., Aharonson et al., 2009; Lora et al., 2014; Lora and Mitchell, 2015) on the actual availability of surface liquids. In other words, without sufficient methane to evaporate into the atmosphere, asymmetric atmospheric transport cannot occur.

The total atmospheric moisture transport is significant, and represents, per Titan year, a northward (or southward under reversed perihelion) mass flux of methane approximately one order of magnitude larger than the mass present in the surface liquids. Of course, this does not correspond to the actual pole-to-pole mass transport, and instead mainly reflects the fact that most of the observable methane on Titan is in the atmosphere. Nevertheless, the atmospheric moisture flux clearly responds to the seasonal asymmetry induced by the orbital configuration.

On the other hand, the latitudinal distributions of differences in atmospheric moisture transport produced by simulations with a reversed longitude of perihelion provide a less consistent picture (Fig. 9). In all cases, these differences are negative at lower latitudes, indicating more southward net transport in the reversed perihelion case, in agreement with the reversed moisture flux asymmetry with reversed seasonal asymmetries. However, the transport differences at the poles are more complicated, again indicating their dependence on the details of the actual surface liquid distribution in each case. Notably, there is either a marginal (Fig. 9a,b) or robust (Fig. 9c) *northward* transport increase at the south pole, suggesting slightly increased *divergence* of methane from the south polar regions under reversed perihelion. In other words, our simulations seem to imply that atmospheric moisture transport out of, rather than into, the southern polar regions would increase if the seasonal asymmetry were reversed. Again, this could reflect the importance of the latitudinal distribution of polar basins, which is different in the two hemispheres.

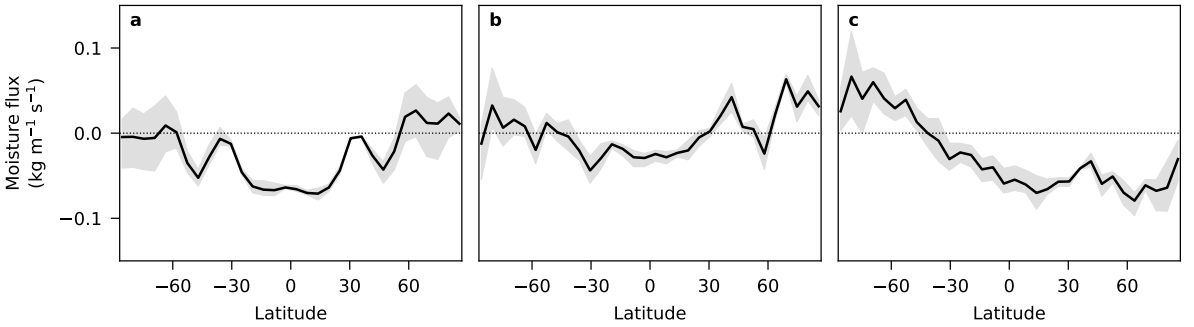


**Figure 9:** Moisture flux differences. Time- and zonal-mean differences in meridional atmospheric moisture flux between the reversed perihelion and modern simulations (a) without topography, (b) with topography, and (c) with topography and increased hydraulic conductivity. In all cases, the gray shading shows the range of decadal averages over the final three decades of the simulations. Positive values indicate northward transport.

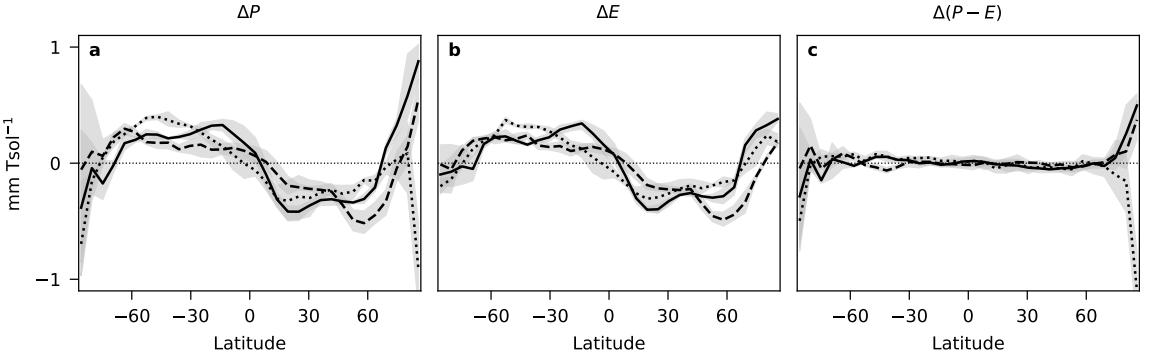


**Figure 10:** Responses of surface fluxes to orbital forcing. Time- and zonal-mean differences in (a) precipitation, (b) evaporation, and (c) precipitation minus evaporation between reversed perihelion and modern simulations. Results are shown for simulations without topography (solid curves), simulations with topography (dashed curves), and simulations with topography and increased hydraulic conductivity (dotted curves). In all cases, the gray shading shows the range of decadal averages over the final three decades of the simulations.

Finally, the precipitation and evaporation responses to reversed perihelion are shown in Fig. 10. In all cases, the global-scale response is the same: reversed perihelion leads to increased (decreased) precipitation in the southern (northern) hemisphere (Fig. 10a), with subtle latitudinal differences that imply a weak dependence on the topography as well as other factors, like the surface liquids, since the simulations with topography but different hydraulic conductivity produce slightly different results. The orbital forcing signal is less clear at the poles, perhaps indicating that stronger cold trapping leads to lower precipitation, but strongly modulated by surface heterogeneity. Notably, precipitation rates over the southern pole are *lower* in the reversed perihelion simulations in all cases, albeit with considerable variability. In addition, the precipitation responses are not very strong: in terms of methane mass, the differences in precipitation are largest at lower latitudes, peaking at magnitudes of $10^{14}$ kg yr$^{-1}$ around 15–45° in both hemispheres; this is orders of magnitude less than total annual precipitation.

As with the responses to topography, the evaporation responses to orbital forcing look very similar to those of the precipitation, except at the poles where evaporation from subsurface methane is important (Fig. 10b). The result is that the net precipitation ($P - E$) response to orbital changes is almost zero everywhere, with noisy responses at the poles (Fig. 10c). Only the case with topography and higher hydraulic conductivity suggests less net precipitation at the northern pole, and then without an accompanying increase in the south. Therefore, while net atmospheric moisture transport robustly reverses with a reversed perihelion (Fig. 8), orbital forcing does *not* produce a clear signal in net precipitation.

In fact, partly as a consequence of the above, surface liquids in our simulations do not show a consistent response to the orbital forcing. This further indicates the importance of the interaction and feedbacks between mechanisms that lead to the distribution of liquids, and their responses to seasonal asymmetries. There is not a simple precipitation or evaporation response in our coupled model that can neatly explain the observed asymmetry of Titan's surface liquids. We conclude that such an asymmetry is likely not a simple expression of orbital forcing, despite the clear atmospheric response to changes in seasonal asymmetries.

## 4. Discussion and Conclusions

With our coupled, self-consistent model of Titan's climate and methane cycle, we have investigated the influence of topography and orbital forcing on the hydroclimate with a series of simulations. Our results show that many mechanisms can contribute to the distribution of surface liquids, and thus to the observed asymmetry of these liquids, in our model. In particular,

- runoff and subsurface hydrology, and the corresponding distribution of basins (a result of topography), are important drivers of the distribution of surface liquids at high latitudes;
- the impact of topography on surface temperatures, as a consequence of the lapse rate, results in the lower-elevation polar regions being warmer, which promotes evaporation and thus, all else being equal, relatively depletes liquids and can eventually throttle the methane cycle;
- relatedly, the rate of replenishment of evaporated liquids from ground methane helps determine whether certain regions dry out or not, but depends, among other things, on the (unknown) hydraulic conductivity;
- topography affects the distribution of precipitation, particularly enhancing mid-latitude precipitation, but only weakly impacts north–south hemispheric contrasts;
- orbital forcing produces a robust response in net atmospheric meridional moisture transport, in agreement with previous results;

- but this transport is also sensitive to other factors and does not unequivocally lead to a strong response of surface liquid distribution to orbital forcing.

Obviously, we do not yet know the details of the hydraulic conductivity of Titan's regolith or the extent and connectivity of the putative methane table, and our results suggest (as in Faulk et al., 2020; Horvath et al., 2016) that these details are important. For example, if the southern pole has lower hydraulic conductivity than does the northern pole, that alone could potentially explain the observed asymmetry, despite the fact that many mechanisms exist that could contribute, as described above. Needless to say, it is possible that other surface heterogeneities or other complications not considered here, as well as model biases, could also play a role. Our simulations qualitatively reproduce the modern methane distribution, but this could be associated with an over-constrained model, which would limit its ability to accurately capture other climate equilibria. What is clear is that any signature of Titan's paleoclimate recorded on the surface may be more difficult to interpret than previously thought, given all of these interacting uncertainties.

Our results demonstrate that Titan's topography plays two major roles in the climate system—through its direct interaction with the atmosphere, and by determining runoff directions and the distribution of basins—but neither depends on significantly asymmetric meridional circulation cells, as is the case, for example, on Mars. At the same time, our results indicate that no glaring inconsistencies with our current understanding of the Titan climate system are introduced by using topography as a boundary condition, lending some further validity to the existing estimates (Corlies et al., 2017). Naturally, improved knowledge of Titan's real topography is essential for future progress, as it would eliminate ambiguities regarding the presence or absence of individual geographical features and enable more targeted regional studies.

Separately, the question of whether or not the northern seas are growing in the present (or shrank in the past) as a consequence of the orbitally-paced global climate remains unresolved. Despite the fact that the atmospheric circulation does, in the net, transport methane northward in the current epoch (as long as there is a sufficient source in the south), this net transport does not cleanly result in surface liquid volume increases in the north relative to the case with reversed perihelion in our model. In all cases examined here, more surface liquid accumulates in the northern hemisphere than the southern by the end of our simulations. This is in agreement with the results of Tokano (2019), albeit for starkly different reasons.

Similarly, only in the simulations with topography and increased hydraulic conductivity is the north–south asymmetry of surface liquids smaller for the reversed perihelion case than for the modern, and even then this is a consequence of more relative loss of the northern seas. In none of our simulations does a reversed perihelion lead to larger southern lakes. If our simulations are representative of Titan, then the southern basins are a relic of a past climate beyond the recent Croll-Milankovitch cycles (Birch et al., 2018), suggesting that Ontario Lacus has not changed

in size significantly in the past tens of millennia (Tokano, 2021) and explaining the lack of evaporites at the south pole (MacKenzie et al., 2014). It does not, however, preclude modest evolution of lake and sea shorelines, which could only be captured by higher resolution or regional models. Thus, whether or not Titan's surface holds intelligible records of millennial climate change remains an open question.

# References


Aharonson, O., Hayes, A.G., Lunine, J.I., Lorenz, R.D., Allison, M.D., Elachi, C., 2009. An asymmetric distribution of lakes on Titan as a possible consequence of orbital forcing. Nature Geosci. 2, 851–854.

Barth, E.L., 2010. Cloud formation along mountain ridges on Titan. Planet. Space Sci. 13, 1740–1747.

Battalio, J.M., Lora, J.M., 2021. Global impacts from high-latitude storms on Titan. Geophys. Res. Lett. 48, e2021GL094244.

Battalio, J.M., Lora, J.M., Rafkin, S., Soto, A., 2021. The interaction of deep convection with the general circulation in Titan's atmosphere. part 2: Impacts on the climate. Icarus 373, 114623.

Birch, S., Hayes, A., Corlies, P., Stofan, E., Hofgartner, J., Lopes, R., Lorenz, R., Lunine, J., MacKenzie, S., Malaska, M., et al., 2018. Morphological evidence that Titan's southern hemisphere basins are paleoseas. Icarus 310, 140–148.

Birch, S., Hayes, A., Dietrich, W., Howard, A., Bristow, C., Malaska, M., Moore, J., Mastrogiuseppe, M., Hofgartner, J., Williams, D., et al., 2017. Geomorphologic mapping of Titan's polar terrains: Constraining surface processes and landscape evolution. Icarus 282, 214–236.

Corlies, P., Hayes, A., Birch, S., Lorenz, R., Stiles, B., Kirk, R., Poggiali, V., Zebker, H., Iess, L., 2017. Titan's Topography and Shape at the End of the Cassini Mission. Geophys. Res. Lett. 44.

Faulk, S.P., Lora, J.M., Mitchell, J.L., Milly, P.C.D., 2020. Titan's climate patterns and surface methane distribution due to the coupling of land hydrology and atmosphere. Nature Astronomy 4, 390–398.

Faulk, S.P., Moon, S., Mitchell, J.L., Lora, J.M., 2017. Regional patterns of extreme precipitation on Titan consistent with observed alluvial fan distribution. Nature Geosci. 10, 827–831.

Griffith, C.A., Rafkin, S., Rannou, P., McKay, C.P., 2014. Storms, clouds, and weather, in: Müller-Wodarg, I., Griffith, C.A., Lellouch, E., Cravens, T.E. (Eds.), Titan: Interior, surface, atmosphere, and space environment. Cambridge University Press, Cambridge, pp. 190–223.

Hayes, A.G., 2016. The lakes and seas of Titan. Ann. Rev. Earth Planet. Sci. 44, 57–83.

Hayes, A.G., Aharonson, O., Lunine, J.I., Kirk, R.L., Zebker, H.A., Wye, L.C., Lorenz, R.D., Turtle, E.P., Paillou, P., Mitri, G., Wall, S.D., Stofan, E.R., Mitchell, K.L., Elachi, C., the Cassini RADAR Team, 2011. Transient surface liquid in Titan's polar regions from Cassini. Icarus 211, 655–671.

Hayes, A.G., Lorenz, R.D., Lunine, J.I., 2018. A post-Cassini view of Titan's methane-based hydrologic cycle. Nature Geosci. 11, 306–313.

Hörst, S.M., 2017. Titan's atmosphere and climate. J. Geophys. Res. Planet. 122.

Horvath, D.G., Andrews-Hanna, J.C., Newman, C.E., Mitchell, K.L., Stiles, B.W., 2016. The influence of subsurface flow on lake formation and north polar lake distribution on Titan. Icarus 277, 103–124.

Jennings, D., Cottini, V., Nixon, C., Achterberg, R., Flasar, F., Kunde, V., Romani, P., Samuelson, R., Mamoutkine, A., Gorius, N., et al., 2016. Surface temperatures on Titan during northern winter and spring. The Astrophysical Journal Letters 816, L17.

Lopes, R.M.C., Wall, S.D., Elachi, C., Birch, S.P.D., Corlies, P., Coustenis, A., Hayes, A.G., Hofgartner, J.D., Janssen, M.A., Kirk, R.L., LeGall, A., Lorenz, R.D., Lunine, J.I., Malaska, M.J., Mastrogiuseppe, M., Mitri, G., Neish, C.D., Notarnicola, C., Paganelli, F., Paillou, P., Poggiali, V., Radebaugh, J., Rodriguez, S., Schoenfeld, A., Soderblom, J.M., Solomonidou, A., Stofan, E.R., Stiles, B.W., Tosi, F., Turtle, E.P., West, R.D.,

Wood, C.A., Zebker, H.A., Barnes, J.W., Casarano, D., Encrenaz, P., Farr, T., Grima, C., Hemingway, D., Karatekin, O., Lucas, A., Mitchell, K.L., Ori, G., Orosei, R., Ries, P., Riccio, D., Soderblom, L.A., Zhang, Z., 2019. Titan as revealed by the Cassini Radar. Space Sci. Rev. 215, 33.

Lora, J.M., Ádámkovics, M., 2017. The near-surface methane humidity on Titan. Icarus 286, 270–279.

Lora, J.M., Lunine, J.I., Russell, J.L., 2015. GCM simulations of Titan's middle and lower atmosphere and comparison to observations. Icarus 250, 516–528.

Lora, J.M., Lunine, J.I., Russell, J.L., Hayes, A.G., 2014. Simulations of Titan's paleoclimate. Icarus 243, 264–273.

Lora, J.M., Mitchell, J.L., 2015. Titan's asymmetric lake distribution mediated by methane transport due to atmospheric eddies. Geophys. Res. Lett. 42, 6213–6220.

Lora, J.M., Tokano, T., Vatant d'Ollone, J., Lebonnois, S., Lorenz, R.D., 2019. A model intercomparison of Titan's climate and low-latitude environment. Icarus 333, 113–126.

Lorenz, R.D., Lopes, R.M., Paganelli, F., Lunine, J.I., Kirk, R.L., Mitchell, K.L., Soderblom, L.A., Stofan, E.R., Ori, G., Myers, M., Miyamoto, H., Radebaugh, J., Stiles, B., Wall, S.D., Wood, C.A., 2008. Titan's inventory of organic surface materials. Geophys. Res. Lett. 35, L02206.

Lorenz, R.D., Stiles, B.W., Aharonson, O., Lucas, A., Hayes, A.G., Kirk, R.L., Zebker, H.A., Turtle, E.P., Neish, C.D., Stofan, E.R., Barnes, J.W., the Cassini RADAR team, 2013. A global topographic map of Titan. Icarus 225, 367–377.

Lunine, J.I., Lorenz, R.D., 2009. Rivers, lakes, dunes, and rain: Crustal processes in Titan's methane cycle. Ann. Rev. Earth Planet. Sci. 37, 299–320.

MacKenzie, S.M., Barnes, J.W., Hofgartner, J.D., Birch, S.P.D., Hedman, M.M., Lucas, A., Rodriguez, S., Turtle, E.P., Sotin, C., 2019a. The case for seasonal surface changes at Titan's lake district. Nature Astronomy 3, 506–510.

MacKenzie, S.M., Barnes, J.W., Sotin, C., Soderblom, J.M., Le Mouélic, S., Rodriguez, S., Baines, K.H., Buratti, B.J., Clark, R.N., Nicholson, P.D., McCord, T.B., 2014. Evidence of Titan's climate history from evaporite distribution. Icarus 243, 191–207.

MacKenzie, S.M., Lora, J.M., Lorenz, R.D., 2019b. A thermal inertia map of Titan. J. Geophys. Res. Planet. 124, 1728–1742.

Mastrogiuseppe, M., Valerio, P., Hayes, A., Lorenz, R., Lunine, J., Picardi, G., Seu, R., Flamini, E., Giuseppe, M., Notarnicola, C., Paillou, P., Zebker, H., 2014. The bathymetry of a Titan sea. Geophys. Res. Lett. 41, 1432–1437.

Mitchell, J.L., 2008. The drying of Titan's dunes: Titan's methane hydrology and its impact on atmospheric circulation. J. Geophys. Res. 113, E08015.

Mitchell, J.L., Lora, J.M., 2016. The climate of Titan. Ann. Rev. Earth Planet. Sci. 44, 353–380.

Neish, C.D., Lorenz, R.D., 2014. Elevation distribution of Titan's craters suggests extensive wetlands. Icarus 228, 27–34.

Newman, C.E., Richardson, M.I., Lian, Y., Lee, C., 2016. Simulating Titan's methane cycle with the TitanWRF general circulation model. Icarus 267, 106–134.

Richardson, M.I., Wilson, R.J., 2002. A topographically forced asymmetry in the martian circulation and climate. Nature 416, 298–301.

Roe, H.G., 2012. Titan's methane weather. Ann. Rev. Earth Planet. Sci. 40, 355–382.

Roe, H.G., Brown, M.E., Schaller, E.L., Bouchez, A.H., Trujillo, C.A., 2005. Geographic control of Titan's mid-latitude clouds. Science 310, 477–479.

Schneider, T., Graves, S.D.B., Schaller, E.L., Brown, M.E., 2012. Polar methane accumulation and rainstorms on Titan from simulations of the methane cycle. Nature 481, 58–61.

Tokano, T., 2019. Orbitally and geographically caused seasonal asymmetry in Titan's tropospheric climate and its implications for the lake distribution. Icarus 317, 337–353.

Tokano, T., 2021. Orbitally forced variation in the size of Ontario Lacus on Titan simulated by a lake balance model. Icarus 354, 114090.

Turtle, E.P., Perry, J.E., Barbara, J.M., Del Genio, A.D., Rodriguez, S., Sotin, C., Lora, J.M., Faulk, S., Corlies, P., Kelland, J., MacKenzie, S.M., West, R.A., McEwen, A.S., Lunine, J.I., Pitesky, J., Ray, T.L., Roy, M., 2018b. Titan's meteorology over the Cassini mission: Evidence for extensive subsurface methane reservoirs. Geophys. Res. Lett. 45, 5320–5328.

Turtle, E.P., Perry, J.E., Hayes, A.G., Lorenz, R.D., Barnes, J.W., McEwen, A.S., West, R.A., Del Genio, A.D., Barbara, J.M., Lunine, J.I., Schaller, E.L., Ray, T.L., Lopes, R.M.C., Stofan, E.R., 2011a. Rapid and extensive surface changes near Titan's equator: Evidence of April showers. Science 331, 1414–1417.

Turtle, E.P., Perry, J.E., Hayes, A.G., McEwen, A.S., 2011b. Shoreline retreat at Titan's Ontario Lacus and Arrakis Planitia from Cassini Imaging Science Subsystem observations. Icarus 212, 957–959.

Zalucha, A.M., Plumb, R.A., Wilson, R.J., 2010. An Analysis of the Effect of Topography on the Martian Hadley Cells. J. Atmos. Sci. 67, 673–693.